This is the accepted manuscript made available via CHORUS. The article has been published as:

Self-contained filtered density function

A. G. Nouri, M. B. Nik, P. Givi, D. Livescu, and S. B. Pope

Phys. Rev. Fluids **2**, 094603 — Published 18 September 2017

DOI: 10.1103/PhysRevFluids.2.094603

A Self-Contained Filtered Density Function

A.G. Nouri, M.B. Nik, and P. Givi

Department of Mechanical Engineering and Materials Science,

University of Pittsburgh,

Pittsburgh, PA 15261, USA

D. Livescu

Los Alamos National Laboratory,

Los Alamos, NM 87544, USA

S.B. Pope

Sibley School of Mechanical and Aerospace Engineering,

Cornell University, Ithaca, NY 14853, USA

(Dated: August 30, 2017)

Abstract

The filtered density function (FDF) closure is extended to a "self-contained" format to include the subgrid scale (SGS) statistics of all of the hydro-thermo-chemical variables in turbulent flows. These are the thermodynamic pressure, the specific internal energy, the velocity vector, and the composition field. In this format, the model is comprehensive and facilitates large eddy simulation (LES) of flows at both low and high compressibility levels. A transport equation is developed for the joint "pressure-energy-velocity-composition filtered mass density function (PEVC-FMDF)." In this equation, the effect of convection appears in closed form. The coupling of the hydrodynamics and thermochemistry is modeled via a set of stochastic differential equation for each of the transport variables. This yields a self-contained SGS closure. For demonstration, LES is conducted of a turbulent shear flow with transport of a passive scalar. The consistency of the PEVC-FMDF formulation is established, and its overall predictive capability is appraised via comparison with direct numerical simulation (DNS) data.

I. INTRODUCTION

The FDF and its density weighted filtered mass density function (FMDF) have proven very effective for LES of turbulent flows [1–8]. The most sophisticated form of the model to-date is one accounting for the joint frequency-velocity-scalar SGS statistics (FVS-FMDF) [9], and a simpler version (VS-FMDF) which does not include the SGS frequency [10–12]. Inclusion of entropy and irreversibility is reported in Refs. [13–15], and extension to multi-phase flows in Refs [16, 17]. Hydrodynamic closure in incompressible, non-reacting flows has been achieved via the marginal velocity-FDF (V-FDF) [18], and the FDF which considers only the species mass fraction field is the scalar-FDF (S-FDF and S-FMDF). This is the most elementary form of the model [19–23], and has experienced widespread applications for LES of a variety of reactive flows. Some examples are in Refs. [24–48]; see Ref. [1] for a recent review. In almost all of these contributions, the FDF is considered for flows at low compressibility levels. As such, the effects of pressure fluctuations in the energy transport is negligible, and the latter is governed by a scalar equation similar to that for the composition. Some corrections to account for the effects of pressure in LES of compressible flows have been attempted [49–51].

The objective of the present work is to extend the FDF methodology to a "self-contained" manner for flows with both low and high levels of compressibility. This is facilitated by SGS modeling of *all* of the pertinent transport variables of compressible flows, as required for a stand-alone description. The central part of the formulation is the "pressure" term which provides the coupling between hydrodynamics and thermochemistry. This term is coupled with the internal energy, the fluid velocity, and the composition field. Consistent with established terminology, the resulting model is termed PEVC-FMDF. With the formal definition of PEVC-FMDF, the mathematical framework for its implementation in LES is established. A transport equation is developed for the PEVC-FMDF in which the effect of the SGS convection appears in closed form. The unclosed terms are modeled via a set of stochastic differential equations (SDEs). Since the FDF is a single-point descriptor, all of the multi-point statistics are also modeled externally. A Lagrangian Monte Carlo procedure is developed and implemented for the numerical solution of these SDEs. Simulations are conducted of a turbulent shear flow with variable levels of compressibility. The consistency and the overall capability of the closure is assessed via comparison with DNS data.

II. FORMULATION

For the mathematical description of compressible flows involving N_s species, the primary transport variables are the density $\rho(\mathbf{x},t)$, velocity vector $u_i(\mathbf{x},t)$ $(i=1,2,3)$, pressure $p(\mathbf{x},t)$, temperature $T(\mathbf{x},t)$, internal energy $e(\mathbf{x},t)$, and species mass fractions $\phi_\alpha(\mathbf{x},t)$ $(\alpha = 1..N_s)$. The equations which govern the transport of the above variables in space (x_i) and time (t) are the continuity, conservation of momentum, internal energy, and species mass fractions:

$$\frac{\partial \rho}{\partial t} + \frac{\partial \rho u_j}{\partial x_j} = 0, \tag{1a}$$

$$\frac{\partial \rho u_i}{\partial t} + \frac{\partial \rho u_i u_j}{\partial x_j} = -\frac{\partial p}{\partial x_i} + \frac{\partial \tau_{ij}}{\partial x_j}, \tag{1b}$$

$$\frac{\partial \rho e}{\partial t} + \frac{\partial \rho e u_j}{\partial x_j} = -\frac{\partial q_j}{\partial x_j} + \sigma_{ij}\frac{\partial u_i}{\partial x_j}, \tag{1c}$$

$$\frac{\partial \rho \phi_\alpha}{\partial t} + \frac{\partial \rho \phi_\alpha u_j}{\partial x_j} = -\frac{\partial J_j^\alpha}{\partial x_j}, \quad \alpha = 1,2,...,N_s. \tag{1d}$$

For a Newtonian fluid, the viscous stress tensor τ_{ij}, the heat flux q_j, the species α diffusive mass flux vector J_j^α, and σ_{ij} tensor are represented by:

$$\tau_{ij} = \mu\left(\frac{\partial u_i}{\partial x_j} + \frac{\partial u_j}{\partial x_i} - \frac{2}{3}\frac{\partial u_k}{\partial x_k}\delta_{ij}\right), \quad q_j = -\lambda\frac{\partial T}{\partial x_j}, \quad J_j^\alpha = -\rho\Gamma_\alpha\frac{\partial \phi_\alpha}{\partial x_j}, \quad \sigma_{ij} = \tau_{ij} - p\delta_{ij}, \tag{2}$$

where μ is the fluid dynamic viscosity, λ is the thermal conductivity, and Γ_α denotes the mass diffusion coefficient. To put the equations in a compact form, and for compatibility with the simulation results presented in the next section, we assume a perfect gas with the specific heat ratio $\gamma = c_p/c_v$, and internal energy $de = c_v dT$; where c_p and c_v denote the specific heats at constant pressure and constant volume, respectively and are assumed to be constants. The diffusion coefficients are the same for all of the species ($\Gamma_\alpha = \Gamma_\beta = \Gamma$); and we assume $\mu = \rho\Gamma$ and $c_v\mu = \lambda$, *i.e.*, unity Schmidt ($Sc = \frac{\mu}{\rho\Gamma}$) and Prandtl ($Pr = \frac{c_v\mu}{\lambda}$) numbers. The viscosity and molecular diffusion coefficients can, in general, be temperature dependent but in this initial study, they are assumed to be constants. In reactive flows, molecular processes and thermodynamics are much more complicated than portrayed here. These are not our primary concern here, so the simple model is adopted with justifications and caveats given in Refs. [52–54]. With these assumptions, the equation of state is expressed as:

$$p = \rho R^0 T/\overline{M} = \rho R T = (\gamma - 1)\rho e, \tag{3}$$

where R^0 and R are the universal and mixture gas constants, and $\overline{M}$ is the molecular weight for the mixture. Therefore, the pressure is governed by [55]:

$$\frac{\partial p}{\partial t}+\frac{\partial p u_j}{\partial x_j}=-\left(\gamma-1\right)\frac{\partial q_j}{\partial x_j}+\left(\gamma-1\right)\sigma_{ij}\frac{\partial u_i}{\partial x_j}. \tag{4}$$

Large eddy simulation involves the spatial filtering operation [56–60]:

$$\langle Q(\mathbf{x},t)\rangle_\ell=\int_{-\infty}^{+\infty}Q(\mathbf{x}',t)G_{\Delta_1}(\mathbf{x}',\mathbf{x})d\mathbf{x}', \tag{5}$$

where $G_{\Delta_1}(\mathbf{x}',\mathbf{x})$ denotes a filter function, and $\langle Q(\mathbf{x},t)\rangle_\ell$ is the filtered value of the transport variable $Q(\mathbf{x},t)$. In this definition, the subscript "1" for the filter function indicates that $\langle Q(\mathbf{x},t)\rangle_\ell$ is the first level filter value of variable $Q(\mathbf{x},t)$ [61]. In variable-density flows, it is convenient to use the Favre-filtered quantity $\langle Q(\mathbf{x},t)\rangle_L=\langle\rho Q\rangle_\ell/\langle\rho\rangle_\ell$. We consider a filter function that is spatially and temporally invariant and localized, thus: $G_{\Delta_1}(\mathbf{x}',\mathbf{x})\equiv G_{\Delta_1}(\mathbf{x}'-\mathbf{x})$ with the properties $G_{\Delta_1}(\mathbf{x})\geq 0$, $\int_{-\infty}^{+\infty}G_{\Delta_1}(\mathbf{x})d\mathbf{x}=1$. Also, the second level spatial filtering operation is defined as:

$$\langle\langle Q(\mathbf{x},t)\rangle_\ell\rangle_{\ell_2}=\int_{-\infty}^{+\infty}\langle Q(\mathbf{x}',t)\rangle_\ell G_{\Delta_2}(\mathbf{x}',\mathbf{x})d\mathbf{x}', \tag{6}$$

where $G_{\Delta_2}(\mathbf{x}',\mathbf{x})$ denotes a secondary filter function. Similar to the first level filtering operation, $\langle\langle Q(\mathbf{x},t)\rangle_L\rangle_{L_2}=\langle\langle\rho Q\rangle_\ell\rangle_{\ell_2}/\langle\langle\rho\rangle_\ell\rangle_{\ell_2}$.

III. PEVC-FMDF

A. Exact transport equation

The PEVC-FMDF, denoted by P_L, is formally defined as [19]:

$$P_L\left(\boldsymbol{v},\boldsymbol{\psi},\theta,\eta,\mathbf{x};t\right)=\int_{-\infty}^{+\infty}\rho(\mathbf{x}',t)\zeta\Big(\boldsymbol{v},\boldsymbol{\psi},\theta,\eta;\boldsymbol{u}(\mathbf{x}',t),\boldsymbol{\phi}(\mathbf{x}',t),e(\mathbf{x}',t),p(\mathbf{x}',t)\Big)G(\mathbf{x}'-\mathbf{x})d\mathbf{x}', \tag{7}$$

where

$$\zeta\Big(\boldsymbol{v},\boldsymbol{\psi},\theta,\eta;\boldsymbol{u}(\mathbf{x},t),\boldsymbol{\phi}(\mathbf{x},t),e(\mathbf{x},t),p(\mathbf{x},t)\Big)=\left(\prod_{i=1}^{3}\delta\left(v_i-u_i(\mathbf{x},t)\right)\right)\times\left(\prod_{\alpha=1}^{\sigma=N_s}\delta\left(\psi_\alpha-\phi_\alpha(\mathbf{x},t)\right)\right)\times\delta\left(\theta-e(\mathbf{x},t)\right)\times\delta\left(\eta-p(\mathbf{x},t)\right), \tag{8}$$

where δ denotes the Dirac delta function, and $\boldsymbol{v}$, $\boldsymbol{\psi}$, θ and η are the velocity vector, composition vector, internal energy and pressure in the sample space. The term ζ is the "fine-grained" density [53, 62]. Equation (7) defines the PEVC-FMDF as the spatially filtered

value of the fine-grained density. With the condition of a positive filter kernel [63], P_L has all of the properties of a mass density function (MDF) [53]. For further developments, it is useful to define the "conditional filtered value" of the variable $Q(\mathbf{x},t)$ as:

$$\Big\langle Q(\mathbf{x},t)\,\Big|\,\boldsymbol{u}(\mathbf{x},t)=\boldsymbol{v},\boldsymbol{\phi}(\mathbf{x},t)=\boldsymbol{\psi},e(\mathbf{x},t)=\theta,p(\mathbf{x},t)=\eta\Big\rangle_L \equiv \Big\langle Q\,\Big|\,\boldsymbol{v},\boldsymbol{\psi},\theta,\eta\,\Big\rangle_L =$$

$$\frac{\int_{-\infty}^{+\infty} Q(\mathbf{x}',t)\rho(\mathbf{x}',t)\zeta\left(\boldsymbol{v},\boldsymbol{\psi},\theta,\eta;\boldsymbol{u}(\mathbf{x}',t),\boldsymbol{\phi}(\mathbf{x}',t),e(\mathbf{x}',t),p(\mathbf{x}',t)\right)G(\mathbf{x}'-\mathbf{x})d\mathbf{x}'}{P_L\left(\boldsymbol{v},\boldsymbol{\psi},\theta,\eta,\mathbf{x};t\right)}. \quad (9)$$

Equation (9) implies the following:

1. For $Q(\mathbf{x},t)=c$:

$$\Big\langle Q(\mathbf{x},t)\,\Big|\,\boldsymbol{v},\boldsymbol{\psi},\theta,\eta\Big\rangle_L = c, \quad (10a)$$

   i.e., the conditional mean of a constant is the constant.

2. For $Q(\mathbf{x},t)\equiv\hat{Q}(\boldsymbol{u}(\mathbf{x},t),\boldsymbol{\phi}(\mathbf{x},t),e(\mathbf{x},t),p(\mathbf{x},t))$:

$$\Big\langle Q(\mathbf{x},t)\,\Big|\,\boldsymbol{v},\boldsymbol{\psi},\theta,\eta\Big\rangle_L = \hat{Q}(\boldsymbol{v},\boldsymbol{\psi},\theta,\eta), \quad (10b)$$

   i.e., the conditional mean of a known function of the dependent variables is simply the function evaluated based on the conditioning (sample-space) variables.

3. Integral properties:

$$\begin{aligned}\langle\rho(\mathbf{x},t)\rangle_\ell\,\langle Q(\mathbf{x},t)\rangle_L &= \langle\rho(\mathbf{x},t)Q(\mathbf{x},t)\rangle_\ell \\ &= \int_{-\infty}^{+\infty}\int_{-\infty}^{+\infty}\Big\langle Q(\mathbf{x},t)\,\Big|\,\boldsymbol{v},\boldsymbol{\psi},\theta,\eta\Big\rangle_L P_L(\boldsymbol{v},\boldsymbol{\psi},\theta,\eta,\mathbf{x};t)d\boldsymbol{v}d\boldsymbol{\psi}d\theta d\eta,\end{aligned} \quad (10c)$$

   i.e., the probability weighted mean of the conditional mean is the unconditional mean.

From Eqs. (10), it follows that the filtered value of any function of the velocity, composition, energy and/or pressure variables is obtained by its integration over the entire sample spaces:

$$\langle\rho(\mathbf{x},t)\rangle_\ell\,\langle Q(\mathbf{x},t)\rangle_L = \int_{-\infty}^{+\infty}\int_{-\infty}^{+\infty}\hat{Q}\left(\boldsymbol{v},\boldsymbol{\psi},\theta,\eta\right)P_L(\boldsymbol{v},\boldsymbol{\psi},\theta,\eta,\mathbf{x};t)d\boldsymbol{v}d\boldsymbol{\psi}d\theta d\eta. \quad (11)$$

The exact transport equation for the PEVC-FMDF is derived by starting with the time derivative of the fine-grained density function:

$$\frac{\partial\zeta}{\partial t} = -\Big(\frac{\partial u_k}{\partial t}\frac{\partial\zeta}{\partial v_k}+\frac{\partial\phi_\alpha}{\partial t}\frac{\partial\zeta}{\partial\psi_\alpha}+\frac{\partial e}{\partial t}\frac{\partial\zeta}{\partial\theta}+\frac{\partial p}{\partial t}\frac{\partial\zeta}{\partial\eta}\Big). \quad (12)$$

Substituting Eqs. (1), Eq. (2), and Eq. (4) into Eq. (12) yields:

$$\frac{\partial \rho\zeta}{\partial t}+\frac{\partial \rho u_j\zeta}{\partial x_j}=\left(\frac{\partial p}{\partial x_j}-\frac{\partial \tau_{kj}}{\partial x_k}\right)\frac{\partial \zeta}{\partial v_j}+\left(\frac{\partial J_j^\alpha}{\partial x_j}\right)\frac{\partial \zeta}{\partial \psi_\alpha}+\Big(\gamma\rho p\frac{\partial u_j}{\partial x_j}+(\gamma-1)\,\rho\frac{\partial q_i}{\partial x_i} - (\gamma-1)\,\rho\tau_{ij}\frac{\partial u_i}{\partial x_j}\Big)\frac{\partial \zeta}{\partial \eta}+\left(\frac{\partial q_i}{\partial x_i}-\tau_{ij}\frac{\partial u_i}{\partial x_j}+p\frac{\partial u_j}{\partial x_j}\right)\frac{\partial \zeta}{\partial \theta}. \tag{13}$$

Integration of this equation according to Eq. (7), while employing Eq. (9) results in:

$$\begin{aligned}\frac{\partial P_L}{\partial t}+\frac{\partial v_j P_L}{\partial x_j}=&\frac{\partial}{\partial v_i}\left(\left\langle\frac{1}{\rho}\frac{\partial p}{\partial x_i}\,\middle|\,\boldsymbol{v},\boldsymbol{\psi},\theta,\eta\right\rangle_L P_L\right)-\frac{\partial}{\partial v_i}\left(\left\langle\frac{1}{\rho}\frac{\partial \tau_{ij}}{\partial x_j}\,\middle|\,\boldsymbol{v},\boldsymbol{\psi},\theta,\eta\right\rangle_L P_L\right)\\&+\frac{\partial}{\partial \psi_\alpha}\left(\left\langle\frac{1}{\rho}\frac{\partial J_j^\alpha}{\partial x_j}\,\middle|\,\boldsymbol{v},\boldsymbol{\psi},\theta,\eta\right\rangle_L P_L\right)+\frac{\partial}{\partial \theta}\left(\left\langle\frac{1}{\rho}\frac{\partial q_i}{\partial x_i}\,\middle|\,\boldsymbol{v},\boldsymbol{\psi},\theta,\eta\right\rangle_L P_L\right)\\&-\frac{\partial}{\partial \theta}\left(\left\langle\frac{1}{\rho}\tau_{ij}\frac{\partial u_i}{\partial x_j}\,\middle|\,\boldsymbol{v},\boldsymbol{\psi},\theta,\eta\right\rangle_L P_L\right)+\frac{\partial}{\partial \theta}\left(\left\langle\frac{1}{\rho}p\frac{\partial u_j}{\partial x_j}\,\middle|\,\boldsymbol{v},\boldsymbol{\psi},\theta,\eta\right\rangle_L P_L\right)\\&+(\gamma-1)\frac{\partial}{\partial \eta}\left(\left\langle\frac{\partial q_i}{\partial x_i}\,\middle|\,\boldsymbol{v},\boldsymbol{\psi},\theta,\eta\right\rangle_L P_L\right)-(\gamma-1)\frac{\partial}{\partial \eta}\left(\left\langle\tau_{ij}\frac{\partial u_i}{\partial x_j}\,\middle|\,\boldsymbol{v},\boldsymbol{\psi},\theta,\eta\right\rangle_L P_L\right)\\&+\gamma\frac{\partial}{\partial \eta}\left(\left\langle p\frac{\partial u_j}{\partial x_j}\,\middle|\,\boldsymbol{v},\boldsymbol{\psi},\theta,\eta\right\rangle_L P_L\right).\end{aligned} \tag{14}$$

This is the exact PEVC-FMDF transport equation in which the effect of convection, the second term on the left-hand side, appears in closed form. The conditional terms on the right hand side are unclosed. The first moments of this equation give the filtered transport equations (with the conventional LES approximation for the diffusion terms) (Eqs. (1)):

$$\frac{\partial \langle\rho\rangle_\ell}{\partial t}+\frac{\partial \langle\rho\rangle_\ell\langle u_j\rangle_L}{\partial x_j}=0, \tag{15a}$$

$$\frac{\partial \langle\rho\rangle_\ell\langle u_i\rangle_L}{\partial t}+\frac{\partial \langle\rho\rangle_\ell\langle u_i\rangle_L\langle u_j\rangle_L}{\partial x_j}=-\frac{\partial \langle p\rangle_\ell}{\partial x_i}+\frac{\partial \breve{\tau}_{ij}}{\partial x_j}-\frac{\partial \langle\rho\rangle_\ell\tau_L(u_i,u_j)}{\partial x_j}, \tag{15b}$$

$$\begin{aligned}\frac{\partial \langle\rho\rangle_\ell\langle e\rangle_L}{\partial t}+\frac{\partial \langle\rho\rangle_\ell\langle u_j\rangle_L\langle e\rangle_L}{\partial x_j}=&-\frac{\partial \breve{q}_j}{\partial x_j}-\frac{\partial \langle\rho\rangle_\ell\tau_L(e,u_j)}{\partial x_j}+\breve{\tau}_{ij}\frac{\partial \langle u_i\rangle_L}{\partial x_j}\\&+\epsilon-\Pi_d-\langle p\rangle_\ell\frac{\partial \langle u_i\rangle_\ell}{\partial x_i},\end{aligned} \tag{15c}$$

$$\frac{\partial \langle\rho\rangle_\ell\langle\phi_\alpha\rangle_L}{\partial t}+\frac{\partial \langle\rho\rangle_\ell\langle u_j\rangle_L\langle\phi_\alpha\rangle_L}{\partial x_j}=-\frac{\partial \breve{J}_j^\alpha}{\partial x_j}-\frac{\partial \langle\rho\rangle_\ell\tau_L(\phi_\alpha,u_j)}{\partial x_j}, \tag{15d}$$

where $\tau_L(a,b)=\langle ab\rangle_L-\langle a\rangle_L\langle b\rangle_L$,

$$\breve{\tau}_{ij}=\mu\left(\frac{\partial \langle u_i\rangle_L}{\partial x_j}+\frac{\partial \langle u_j\rangle_L}{\partial x_i}-\frac{2}{3}\frac{\partial \langle u_k\rangle_L}{\partial x_k}\delta_{ij}\right),\quad \breve{q}_j=-\lambda\frac{\partial \langle T\rangle_L}{\partial x_j},\quad \breve{J}_j^\alpha=-\langle\rho\rangle_\ell\,\Gamma\frac{\partial \langle\phi_\alpha\rangle_L}{\partial x_j}, \tag{16}$$

and Π_d and ϵ denote the SGS pressure dilatation and dissipation, respectively:

$$\Pi_d=\left\langle p\frac{\partial u_i}{\partial x_i}\right\rangle_\ell-\langle p\rangle_\ell\frac{\partial \langle u_i\rangle_\ell}{\partial x_i},\quad \epsilon=\left\langle\tau_{ij}\frac{\partial u_i}{\partial x_j}\right\rangle_\ell-\breve{\tau}_{ij}\frac{\partial \langle u_i\rangle_L}{\partial x_j}. \tag{17}$$

B. Modeled transport equation

To develop the model for the PEVC-FMDF, the notion of "stochastic" particles [56] is used. This is via development of SDEs governing the FDF transport variables: U_i^+, ϕ_α^+, E^+, and P^+. The internal energy is modeled according to the first law of thermodynamics:

$$dE^+ = \Big(- C_e\Omega \left[E^+ - \langle e\rangle_L\right] + \frac{E^+(\gamma-1)}{P^+}\epsilon\Big)dt - P^+ d\xi^+, \tag{18}$$

where C_e is the model constant, Ω denotes the SGS mixing frequency, and $\xi^+ = 1/\rho^+$ is the specific volume relating E^+ and P^+ through the equation of state. In the context of single-point formulation both of these variables need closures. In the absence of better alternatives, the simple models suggested in the previous work [9] are adopted:

$$\epsilon = \langle\rho\rangle_\ell C_\epsilon k^{3/2}/\Delta_L,\ \Omega = \epsilon/(\langle\rho\rangle_\ell k), \tag{19}$$

here C_ϵ is the model constant, Δ_L is the LES filter size and $k = \frac{1}{2}\tau_L(u_i,u_i)$ is the SGS kinetic energy. The pressure SDE is written in the general form:

$$dP^+ = P^+\left(Adt + BdW_p\right), \tag{20}$$

where $W_p(t)$ denotes the Wiener process [64]. With this, the energy SDE takes the form:

$$\begin{aligned} dE^+ = \Big(&- \frac{C_e\Omega}{\gamma}\left(E^+ - \langle e\rangle_L\right) + \frac{\gamma-1}{\gamma}\frac{E^+}{P^+}\epsilon + \frac{\gamma-1}{\gamma}E^+\left(A - \frac{B^2}{\gamma}\right)\Big)dt \\ &+ \frac{\gamma-1}{\gamma}E^+ B dW_p. \end{aligned} \tag{21}$$

The coefficients A and B are determined so that the exact and modeled transport equations for energy are identical, and the filtered specific volume is consistently determined by the FDF and the equation of state. There are different combinations of A and B that satisfy these constraints. To ensure realizability, we select the model [65, 66]:

$$A = \frac{\epsilon(\gamma-1)}{P^+} - \gamma\frac{\partial\langle u_j\rangle_\ell}{\partial x_j} + \varkappa_P(\gamma-1)(P^+ - \langle p\rangle_\ell) + \gamma\frac{\partial}{\partial x_j}\left(\mu\frac{\partial}{\partial x_j}\left(\frac{1}{\langle\rho\rangle_\ell}\right)\right), \tag{22}$$

$$B = 0, \tag{23}$$

with:

$$\varkappa_P = \frac{\gamma}{(\gamma-1)\tau_\ell(p,p)}\left(\breve{\tau_{ij}}\frac{\partial\langle u_i\rangle_L}{\partial x_j} - \mathcal{F}_d - \langle p\rangle_\ell\frac{\partial}{\partial x_j}\left(\mu\frac{\partial}{\partial x_i}\left(\frac{1}{\langle\rho\rangle_\ell}\right)\right)\right), \tag{24}$$

where $\mathcal{F}_d$ is the general form of the model for the pressure dilatation based on known SGS statistics. For modeling of the other variables, we follow Refs. [12, 18, 22, 67, 68] and use the simplified Langevin model (SLM) and linear mean-square estimation (LMSE) model [69]:

$$dX_i^+ = U_i^+ dt + \sqrt{\frac{2\mu}{\langle\rho\rangle_\ell}} dW_i, \tag{25a}$$

$$\begin{aligned} dU_i^+ = &-\frac{1}{\langle\rho\rangle_\ell}\frac{\partial\langle p\rangle_\ell}{\partial x_i}dt + \frac{2}{\langle\rho\rangle_\ell}\frac{\partial}{\partial x_j}\left(\mu\frac{\partial\langle u_i\rangle_L}{\partial x_j}\right)dt + \frac{1}{\langle\rho\rangle_\ell}\frac{\partial}{\partial x_j}\left(\mu\frac{\partial\langle u_j\rangle_L}{\partial x_i}\right)dt \\ &- \frac{2}{3}\frac{1}{\langle\rho\rangle_\ell}\frac{\partial}{\partial x_i}\left(\mu\frac{\partial\langle u_j\rangle_L}{\partial x_j}\right)dt + G_{ij}\left(U_j^+ - \langle u_j\rangle_L\right)dt + \sqrt{C_0\frac{\epsilon}{\langle\rho\rangle_\ell}}dW_i' \\ &+ \sqrt{\frac{2\mu}{\langle\rho\rangle_\ell}}\frac{\partial\langle u_i\rangle_L}{\partial x_j}dW_j, \end{aligned} \tag{25b}$$

$$d\phi_\alpha^+ = -C_\phi\Omega\left(\phi_\alpha^+ - \langle\phi_\alpha\rangle_L\right)dt, \tag{25c}$$

where $\mathbf{W}$, $\mathbf{W}'$ denote the Wiener process in the physical and the velocity spaces, respectively, and:

$$G_{ij} = \left(\frac{\Pi_d}{2k\langle\rho\rangle_\ell} - \Omega\left(\frac{1}{2} + \frac{3}{4}C_0\right)\right)\delta_{ij}, \tag{26}$$

in which we employ the model:

$$\Pi_d = C_\Pi\left(\left\langle\langle p\rangle_\ell\frac{\partial\langle u_i\rangle_L}{\partial x_i}\right\rangle_{\ell_2} - \langle\langle p\rangle_\ell\rangle_{\ell_1}\frac{\partial\langle\langle u_i\rangle_L\rangle_{L_2}}{\partial x_i}\right). \tag{27}$$

The parameters C_0, C_ϕ, and C_Π are the model constants and needed to be specified [11, 70]. The Fokker-Planck equation [71], governing the joint probability density function of the SGS transport parameters is:

$$\begin{aligned} \frac{\partial F_L}{\partial t} + \frac{\partial v_i F_L}{\partial x_i} = &\frac{1}{\langle\rho\rangle_\ell}\frac{\partial\langle p\rangle_\ell}{\partial x_i}\frac{\partial F_L}{\partial v_i} - \frac{2}{\langle\rho\rangle_\ell}\frac{\partial}{\partial x_j}\left(\mu\frac{\partial\langle u_i\rangle_L}{\partial x_j}\right)\frac{\partial F_L}{\partial v_i} - \frac{1}{\langle\rho\rangle_\ell}\frac{\partial}{\partial x_j}\left(\mu\frac{\partial\langle u_j\rangle_L}{\partial x_i}\right)\frac{\partial F_L}{\partial v_i} \\ &+ \frac{2}{3}\frac{1}{\langle\rho\rangle_\ell}\frac{\partial}{\partial x_i}\left(\mu\frac{\partial\langle u_j\rangle_L}{\partial x_j}\right)\frac{\partial F_L}{\partial v_i} - \frac{\partial\left(G_{ij}\left(v_j - \langle u_j\rangle_L\right)F_L\right)}{\partial v_i} + \frac{\partial}{\partial x_i}\left(\mu\frac{\partial(F_L/\langle\rho\rangle_\ell)}{\partial x_i}\right) \\ &+ \frac{\partial}{\partial x_i}\left(\frac{2\mu}{\langle\rho\rangle_\ell}\frac{\partial\langle u_j\rangle_L}{\partial x_i}\frac{\partial F_L}{\partial v_j}\right) + \frac{\mu}{\langle\rho\rangle_\ell}\frac{\partial\langle u_k\rangle_L}{\partial x_j}\frac{\partial\langle u_i\rangle_L}{\partial x_j}\frac{\partial^2 F_L}{\partial v_k\partial v_i} + \frac{1}{2}C_0\frac{\epsilon}{\langle\rho\rangle_\ell}\frac{\partial^2 F_L}{\partial v_i\partial v_i} \\ &+ C_\phi\Omega\frac{\partial\left(\left(\psi_\alpha - \langle\phi_\alpha\rangle_L\right)F_L\right)}{\partial\psi_\alpha} + \frac{C_e\Omega}{\gamma}\frac{\partial\left(\left(\theta - \langle e\rangle_L\right)F_L\right)}{\partial\theta} - \frac{\gamma-1}{\gamma}(\epsilon)\frac{\partial}{\partial\theta}\left(\frac{\theta}{\eta}F_L\right) \\ &- \frac{\gamma-1}{\gamma}\frac{\partial\left(\theta A F_L\right)}{\partial\theta} + \frac{\gamma-1}{\gamma^2}\frac{\partial\left(\theta B^2 F_L\right)}{\partial\theta} - \frac{\partial\left(\eta A F_L\right)}{\partial\eta} + \frac{1}{2}\frac{(\gamma-1)^2}{\gamma^2}\frac{\partial^2\left(\theta^2 B^2 F_L\right)}{\partial\theta\partial\theta} \\ &+ \frac{\gamma-1}{\gamma}\frac{\partial^2\left(\theta\eta B^2 F_L\right)}{\partial\theta\partial\eta} + \frac{1}{2}\frac{\partial^2\left(\eta^2 B^2 F_L\right)}{\partial\eta\partial\eta}. \end{aligned} \tag{28}$$

The transport equations for the first-order moments are obtained by integration of Eq. (28) according to Eqs. (10).

IV. NUMERICAL SOLUTION

The modeled PEVC-FMDF transport equation is solved by a hybrid finite-difference (FD) / Monte Carlo (MC) method, similar to those in previous works [3, 72]. The FDF is represented by an ensemble of MC particles, each carrying the information pertaining to its position $\mathbf{X}^+$, velocity $\boldsymbol{U}^+$, composition $\boldsymbol{\phi}^+$, energy E^+, and pressure P^+. We define the $\boldsymbol{Z}^+(t)$, a $8+N_s$ vector, as:

$$\boldsymbol{Z}^+(t) = [\mathbf{X}^+(t), \boldsymbol{U}^+(t), \boldsymbol{\phi}^+(t), E^+(t), P^+(t)], \tag{29}$$

which evolves by:

$$d\boldsymbol{Z}^+ = \boldsymbol{D}(\boldsymbol{Z}^+)dt + \boldsymbol{B}(\boldsymbol{Z}^+)d\boldsymbol{W}, \tag{30}$$

where $\boldsymbol{W}$ is the Wiener-Levy vector, and the matrices $\boldsymbol{D}$ and $\boldsymbol{B}$ can be identified from Eqs. (18),(20), and (25). The vector $\boldsymbol{Z}$ is updated via the Euler-Maruyama discretization [73]:

$$\boldsymbol{Z}^+(t_{k+1}) = \boldsymbol{Z}^+(t_k) + \boldsymbol{D}\left(\boldsymbol{Z}^+(t_k)\right)\Delta t + \boldsymbol{B}\left(\boldsymbol{Z}^+(t_k)\right)\Delta t^{1/2}\zeta_k, \tag{31}$$

where ζ_k is an independent standardized Gaussian random variable at time t_k, and Δt is the time step. This scheme preserves the Markovian character of the diffusion processes and the Itô-Gikhman character of the SDEs [74].

The computational domain is discretized on equally-spaced FD grid points. These are used to identify the regions where the statistical information are to be obtained, and to perform complementary LES solely by FD discretization. The latter is referred to as LES-FD and is useful for assessing the consistency of the MC solver. In this solver, the statistical information is obtained by considering an ensemble of N_E MC particles residing within a cubic domain of side Δ_E centered around each of the FD points. For reliable statistics with minimal numerical dispersion, it is desired to minimize the size of the ensemble domain and maximize the number of the MC particles [53]. In this way:

$$\begin{aligned}
\langle a \rangle_E &\equiv \frac{\sum_{n\in\Delta_E} w^{(n)} a^{(n)}}{\sum_{n\in\Delta_E} w^{(n)}} \xrightarrow[\substack{N_E\to\infty \\ \Delta_E\to 0}]{} \langle a \rangle_L \,, \\
\tau_E(a,b) &\equiv \left(\frac{\sum_{n\in\Delta_E} w^{(n)} a^{(n)} b^{(n)}}{\sum_{n\in\Delta_E} w^{(n)}} \right) - \langle a \rangle_E \langle b \rangle_E \xrightarrow[\substack{N_E\to\infty \\ \Delta_E\to 0}]{} \tau_L(a,b) \,,
\end{aligned} \tag{32}$$

where $w^{(n)}$ is the weight of the n^{th} MC particle and $a^{(n)}$ denotes the information carried by that particle pertaining to transport variable a. The LES-FD solver is based on the

second-order predictor-corrector scheme. All of the FD operations are conducted on fixed grid points. The transfer of information from these points to the MC particles is via a trilinear interpolation. The transfer of information from the particles to the grid points is by means of ensemble averaging. The transport equations to be solved by the LES-FD include unclosed second-order moments which are obtained from the MC. The LES-FD also determines the filtered values of the transport variables. This redundancy is useful in monitoring the accuracy and consistency of the FDF results [18, 72, 75].

V. RESULTS

A. Flow and numerical specifications

Simulations are conducted of a three-dimensional (3D) temporally developing mixing layer involving the transport of a passive scalar. The temporal layer consists of two parallel streams traveling in opposite directions with the same speed [20, 76–78]. The LES predictions are compared with direct numerical simulation (DNS) data of the same layer. In this layer, x, y and z denote the streamwise, the cross-stream, and the spanwise directions, respectively. The velocity components along these directions are denoted, in order, by u, v and w. The transport variables are normalized with respect to the half initial vorticity thickness, $L_r = \frac{\delta_v(t=0)}{2}$. Here, $\delta_v = \frac{\Delta U}{|\partial \overline{\langle u \rangle}_L / \partial y|_{max}}$, where $\overline{\langle u \rangle}_L$ is the Reynolds-averaged value of the filtered streamwise velocity and ΔU is the velocity difference across the layer. The length L_v is specified such that $L_v = 2^{N_P} \lambda_u$, where N_P is the desired number of successive vortex pairings and λ_u is the wavelength of the most unstable mode corresponding to the mean streamwise velocity profile imposed at the initial time. The normalized filtered streamwise velocity, the scalar composition and the temperature are initialized with a hyperbolic tangent profiles with $\langle u \rangle_L = 1$, $\langle \phi \rangle_L = 1$ on the top stream, and $\langle u \rangle_L = -1$, $\langle \phi \rangle_L = 0$ on the bottom stream. With a constant initial pressure, the parameter "s" denotes the initial density ratio across the layer; the values $s = 1,\ 2,\ 4$ are considered. The reference velocity is $U_r = \Delta U/2$. The Reynolds number is set ($Re = \frac{U_r L_r}{\nu}$) $= 50$, and the Mach numbers ($Ma = \frac{U_r}{\sqrt{\gamma R T_r}}$) values of 0.2, 0.6 and 1.2 are considered. The number of test cases and the magnitude of the Reynolds number, as considered, are based on the amount of available computational resources.

The 3D field is initialized in a procedure somewhat similar to that in Ref. [78]. The formation of the large scale structures are expedited through eigenfunction based initial perturbations. This includes 2D and 3D perturbations with a random phase shift between the modes. This yields the formation of two successive vortex pairings and strong three-dimensionality. Periodic boundary conditions are imposed in the homogeneous directions (x and z), and characteristic boundary conditions [79] are employed in the cross-stream direction. Simulations are conducted on a box, $0 \leq x \leq L$, $\frac{-3L}{2} \leq y \leq \frac{3L}{2}$, $0 \leq z \leq L$ where $L = L_v/L_r$. The layer is discretized with nearly equally-spaced grid points ($\Delta y \cong \Delta x = \Delta z$) with the number of grid points $193 \times 577 \times 193$ for DNS, and $65 \times 193 \times 65$ for LES. Some lower resolution LES $33 \times 97 \times 33$ were also conducted for production runs. The resolution in LES was determined in such a way that a reasonable amount ($75\% - 85\%$) of turbulent energy is captured by the resolved scale. To filter the DNS data, a top-hat function is used with $\Delta_L = 2\,\Delta$, where $\Delta = (\Delta x \Delta y \Delta z)^{1/3}$. The LES filter sizes are $\Delta_1 = \Delta_L$ and $\Delta_2 = 2\Delta_L$. No attempt is made to investigate the sensitivity of the results to the filter function [63] or the size of the filter [80–82].

The MC particles are initially distributed uniformly within the domain in a random fashion. The particle weights, $w^{(n)}$, are set according to filtered fluid density at the initial time. The initial number of particles per grid point is $NPG = 80$, and the ensemble domain size (Δ_E) is set equal to the grid spacing. The effects of both of these parameters have been assessed in previous works [11, 18, 22, 23]. All results are analyzed both "instantaneously" and "statistically." In the former, the instantaneous scatter plots of the variables of interest are analyzed. In the latter, the "Reynolds-averaged" statistics constructed from the instantaneous data are considered. These are constructed by spatial averaging over homogeneous directions. All Reynolds-averaged results are denoted by an overbar. No attempt is made to determine the optimum magnitudes of the model constants. The values as suggested in the literature are adopted for $C_0 = 2.1$, and $C_\phi = C_\epsilon = 1$ [11, 83]. The values of $C_\Pi = 1$ and $C_e = 1.4$ were chosen based on comparison with DNS data for one set of the simulations, and were used in all the subsequent ones.

B. Consistency and validity assessments

To demonstrate consistency, the redundancy of the repeated fields is portrayed by scatter plots of the instantaneous values. The accuracy of the LES-FD is relatively well-established

(at least for the first-order filtered quantities), thus the comparative assessment provides a good measure of the MC performance. Sample results are given in Fig. 1, and portray a reasonable consistency.

For comparison with DNS data, the resolved and the "total" components of the Reynolds-averaged moments are considered. The former is denoted by $\overline{R(a,b)}$, with $R(a,b) = \left(\langle a\rangle_L - \overline{\langle a\rangle_L}\right)\left(\langle b\rangle_L - \overline{\langle b\rangle_L}\right)$, and the latter by $\overline{r(a,b)}$, with $r(a,b) = (a-\overline{a})\left(b-\overline{b}\right)$; In DNS, the total components are directly available, while in LES they are approximated via $\overline{r(a,b)} \approx \overline{R(a,b)} + \overline{\tau_L(a,b)}$ [55].

Figure 2 shows the instantaneous iso-surfaces of the composition field $\langle\phi\rangle_L$ obtained by PEVC-FMDF for $Ma = 0.2$ at $t = 50$ and $Ma = 1.2$ at $t = 75$. By these times, the flows have gone through pairings and exhibit strong 3D effects. This is evident by the formation of large scale spanwise rollers with the presence of secondary structures in streamwise planes [84].

Figure 3 shows the Reynolds-averaged, filtered density and streamwise velocity fields. The level of agreement between PEVC-FMDF and DNS is satisfactory. Similar agreements are observed for all other filtered variables. The figure is also indicative of the accurate prediction of shear layer center location by PEVC-FMDF. As the density ratio increases, the shear layer center, defined as the dividing mean streamline position (the position where $\overline{\langle u\rangle_L}$ is equal to the average of the free stream velocities), is shifted further to the low-density side. As a result, the peak values of the Reynolds stresses and scalar fluxes also show a shift to the low-density side. The shift is known to be responsible for the decreased correlation between density and velocity components [85] and hence, reduction in turbulent production terms. The growth rate of the later is related to the integrated turbulent production [86]. Therefore, a decrease in this production results in reduction of the layer growth rate. This is evidenced in Fig. 4 which shows the temporal evolution of the momentum thickness (δ_m) [63]. As Fig. 4 shows, the shear layer growth rate reduces with increasing the density ratio, and increasing the Ma number. This is consistent with previous DNS results [20, 76, 87]. However, the spreading rates as predicted by the FDF are somewhat smaller than those by DNS. This was also observed in previous FDF simulations [9].

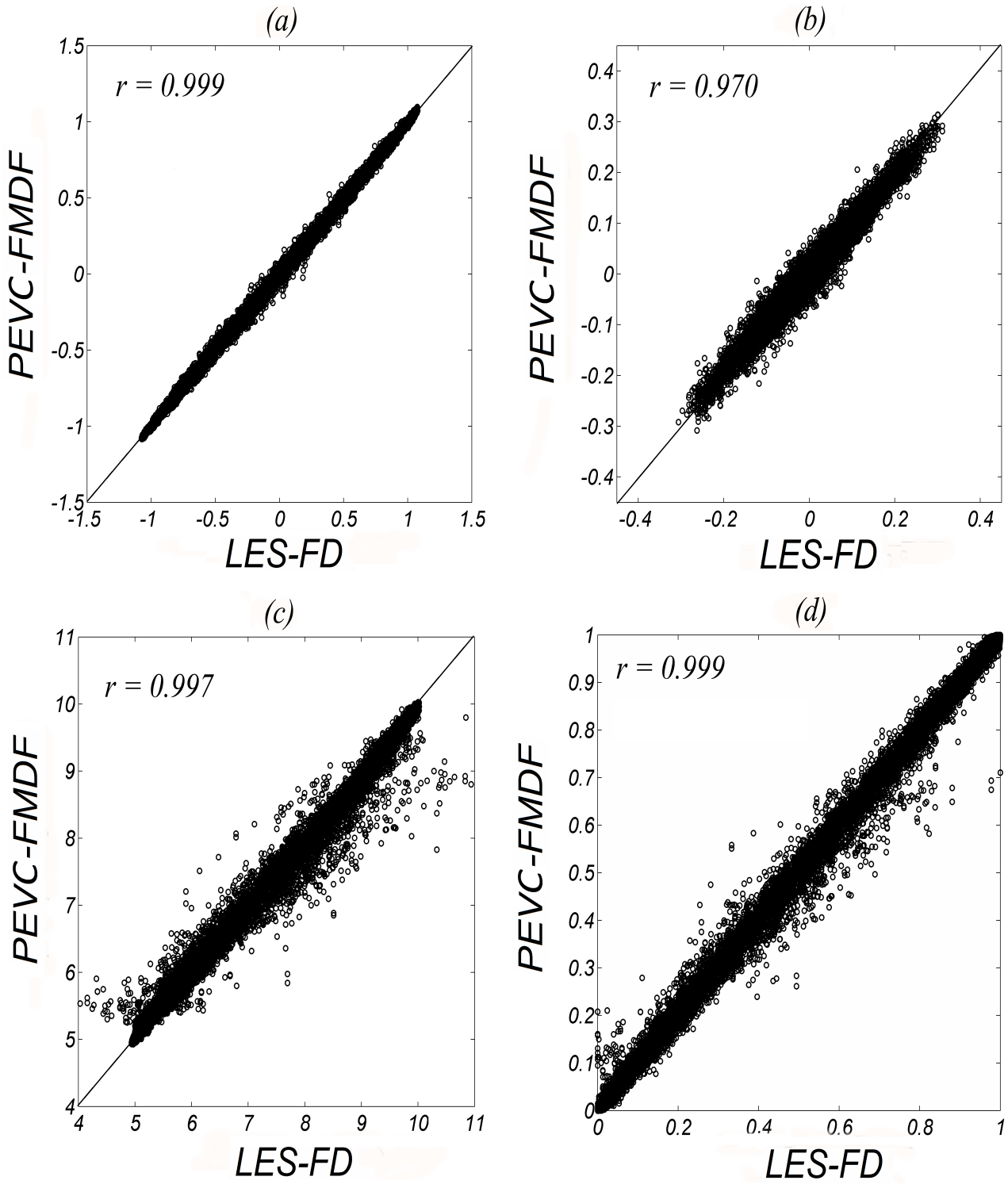

FIG. 1: Scatter plots of (a) $\langle u \rangle_L$, (b) $\langle v \rangle_L$, (c) $\langle e \rangle_L$, and (d) $\langle \phi \rangle_L$, with $Ma = 0.6$ and $s = 2$ at $t = 45$. r denotes the correlation coefficient.

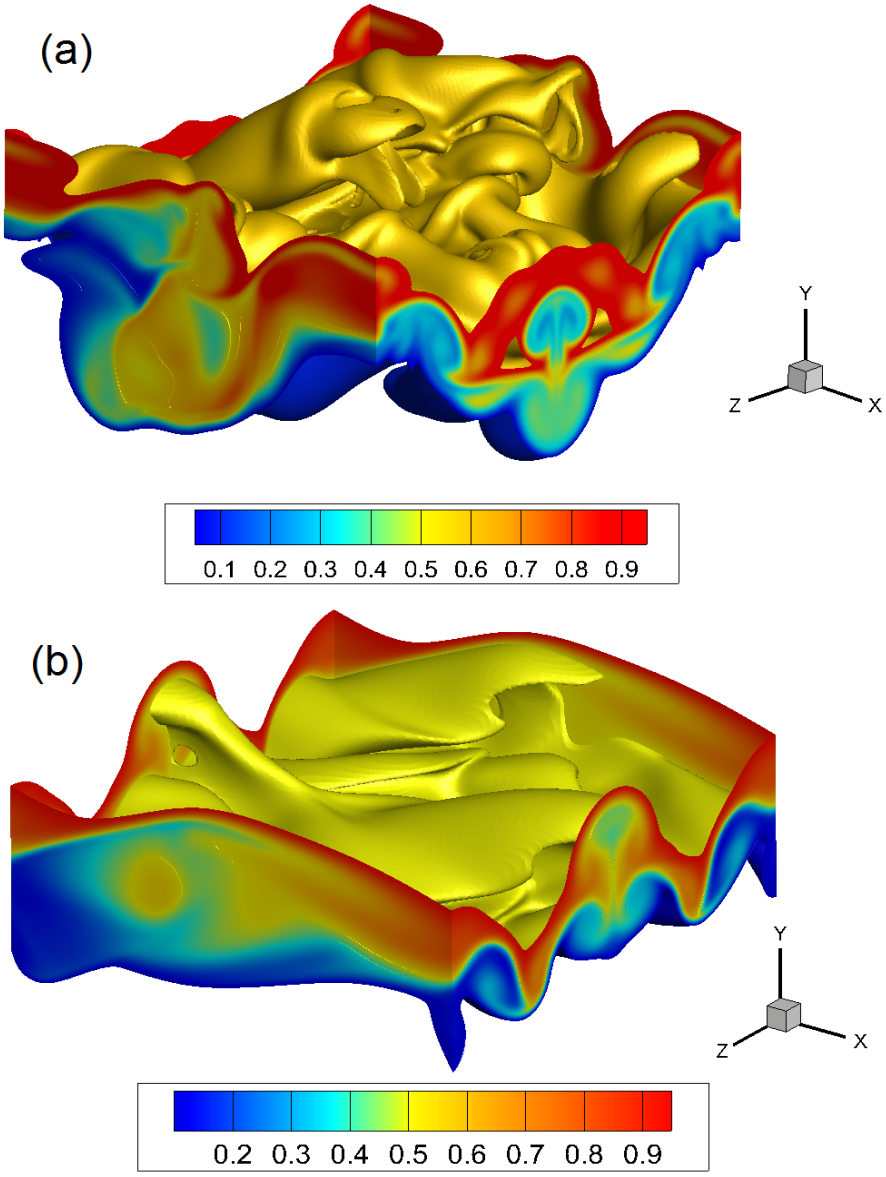

FIG. 2: Contour surfaces of the instantaneous $\langle\phi\rangle_L$ field. (a) $Ma = 0.2$, $s = 2$ and $t = 50$, (b) $Ma = 1.2$, $s = 2$ and $t = 75$.

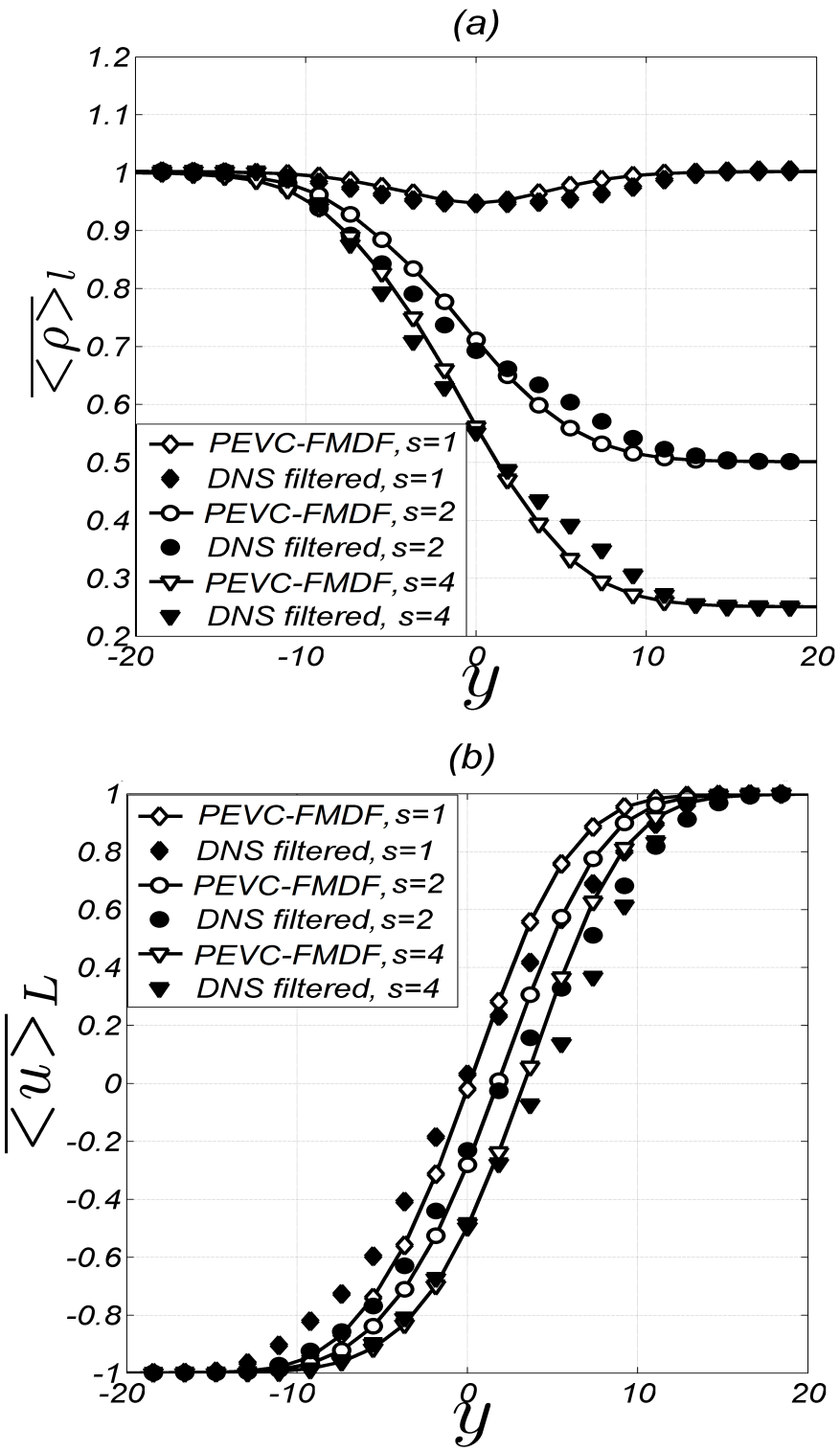

FIG. 3: Cross-stream variation of Reynolds-averaged (a) $\overline{\langle\rho\rangle_\ell}$ and (b) $\overline{\langle u\rangle_L}$ with $Ma = 0.6$ at $t = 45$.

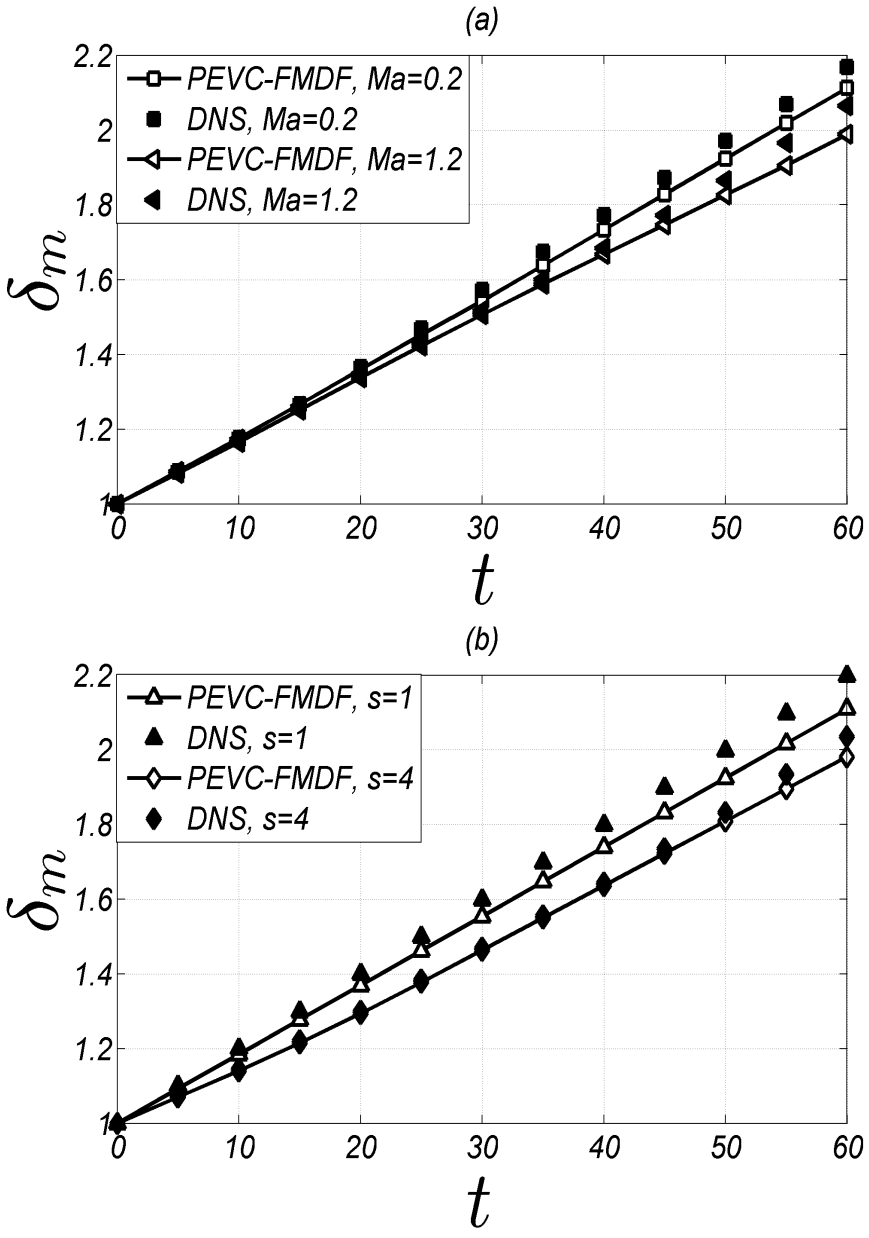

FIG. 4: Temporal variation of the normalized momentum thickness. (a) $s = 2$ (b) $Ma = 1.2$.

Several components of the resolved second-order resolved and SGS moments are presented in Figs. 5, 8,and 11. As observed, the PEVC-FMDF yields reasonable predictions. As a result, the total components also yield very good agreements with DNS data as shown in Figs. 7, 10, and 13.

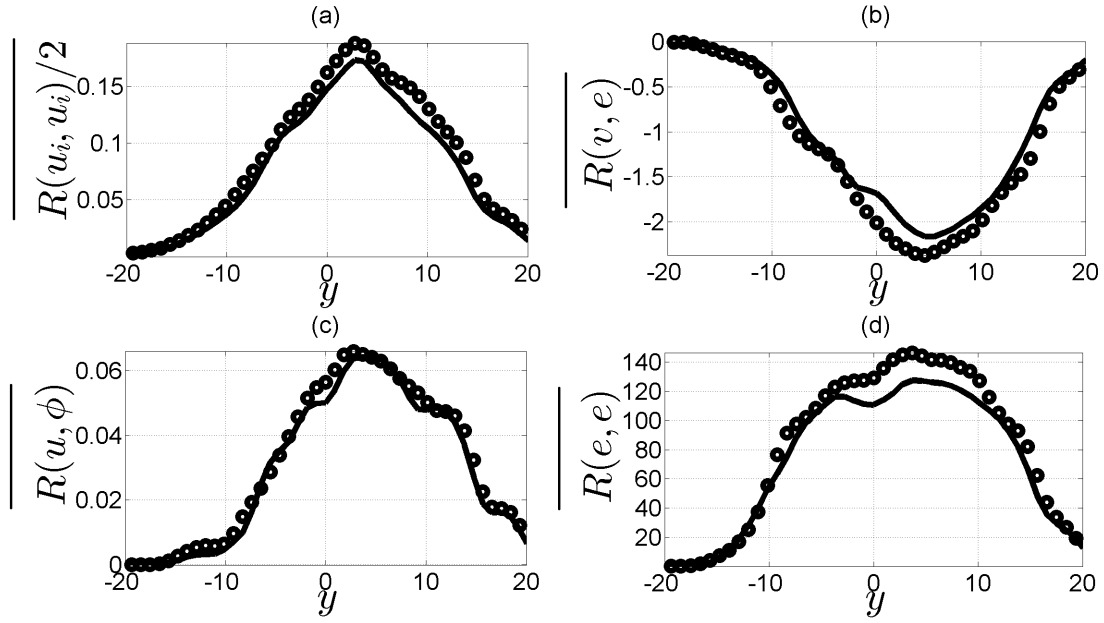

FIG. 5: Cross-stream variation of some of the components of $\overline{R}$ at $t = 50$ with $Ma = 0.2$ and $s = 2$. The thick solid line denote LES predictions using PEVC-FMDF and circles show the DNS data.

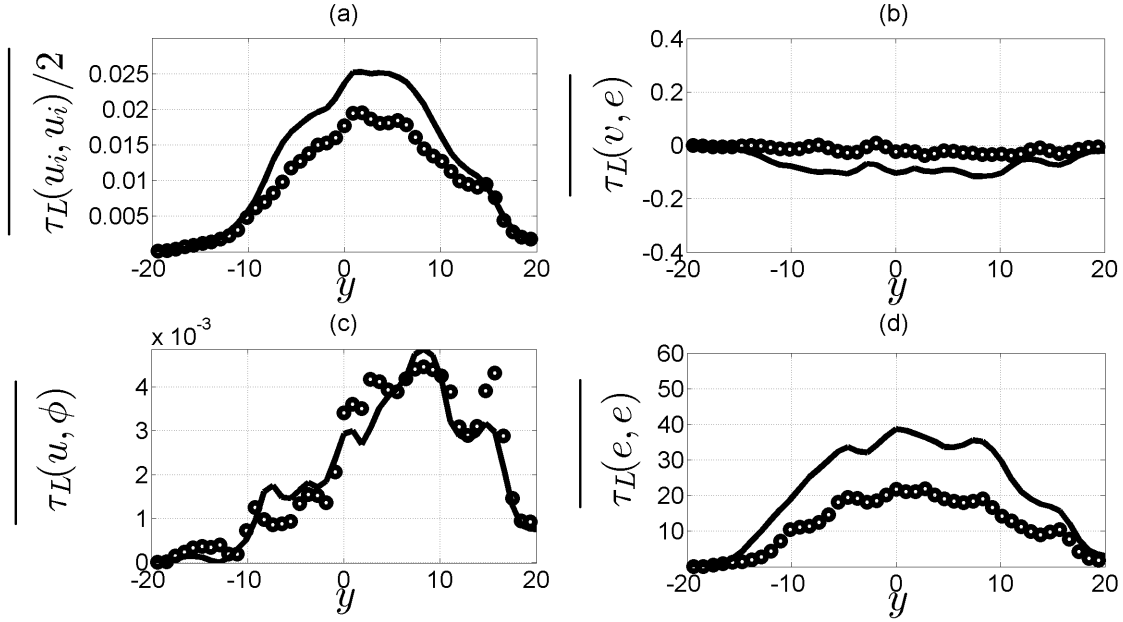

FIG. 6: Cross-stream variation of some of the Reynolds-averaged components of $\overline{\tau_L}$ at $t = 50$ with $Ma = 0.2$ and $s = 2$. The thick solid line denote LES predictions using PEVC-FMDF and circles show the DNS data.

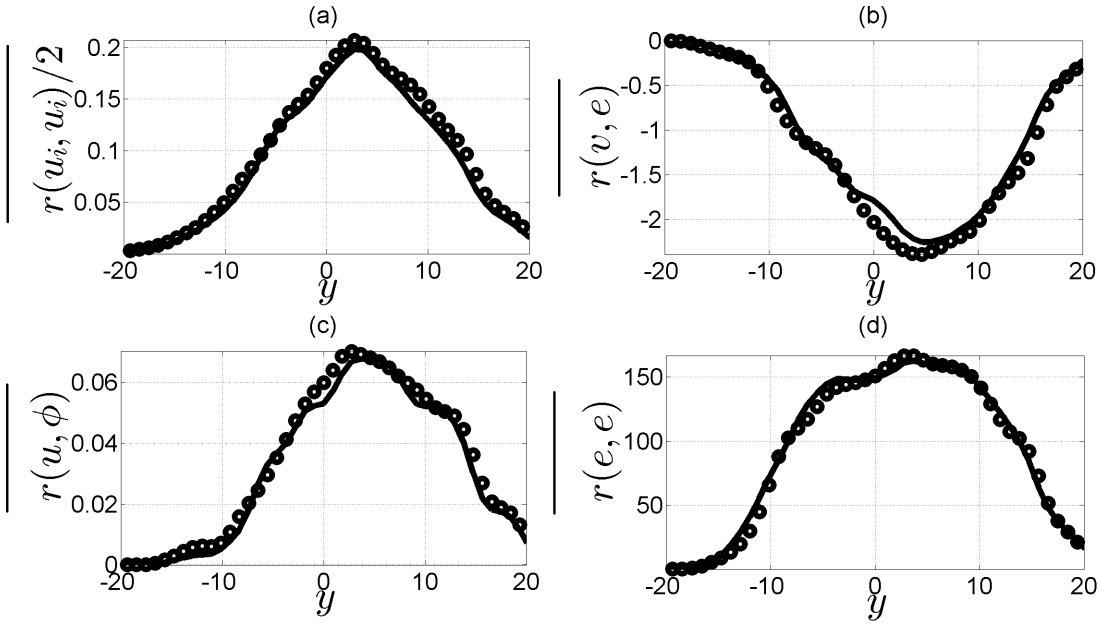

FIG. 7: Cross-stream variation of some of the components of $\overline{r}$ at $t = 50$ with $Ma = 0.2$ and $s = 2$. The thick solid line denote LES predictions using PEVC-FMDF and circles show the DNS data.

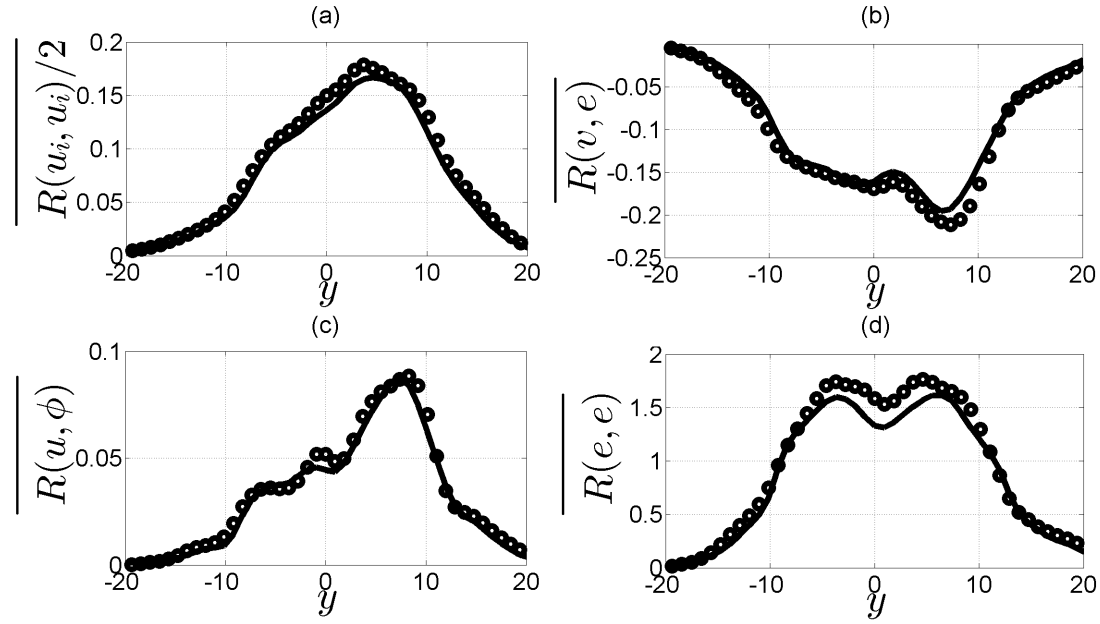

FIG. 8: Cross-stream variation of some of the components of $\overline{R}$ at $t = 65$ with $Ma = 0.6$ and $s = 2$. The thick solid line denote LES predictions using PEVC-FMDF and circles show the DNS data.

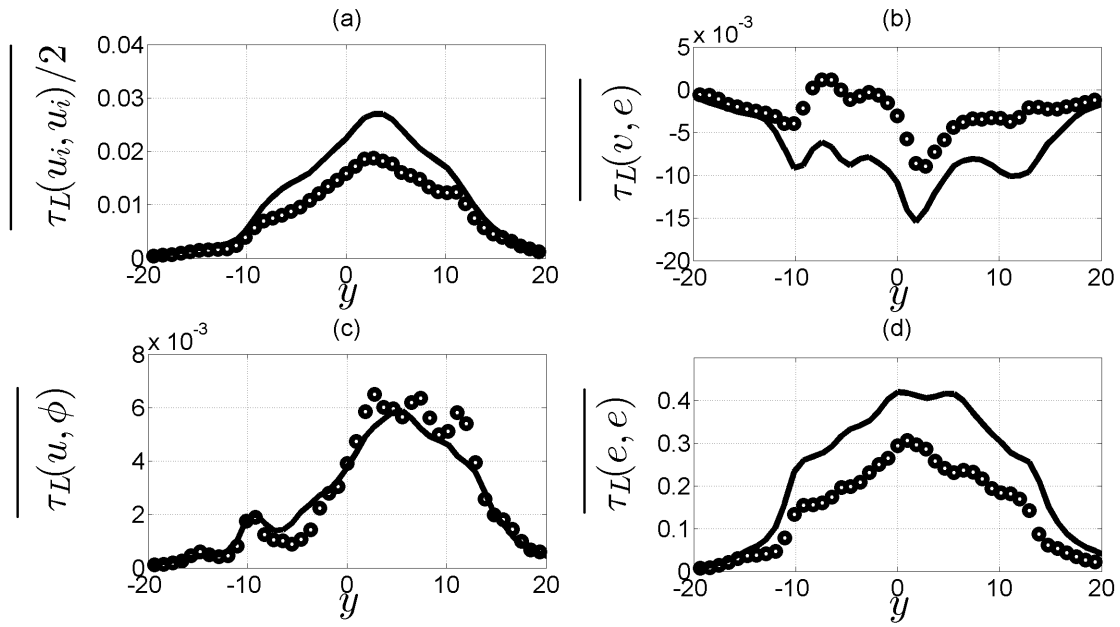

FIG. 9: Cross-stream variation of some of the Reynolds-averaged components of $\overline{\tau_L}$ at $t = 65$ with $Ma = 0.6$ and $s = 2$. The thick solid line denote LES predictions using PEVC-FMDF and circles show the DNS data.

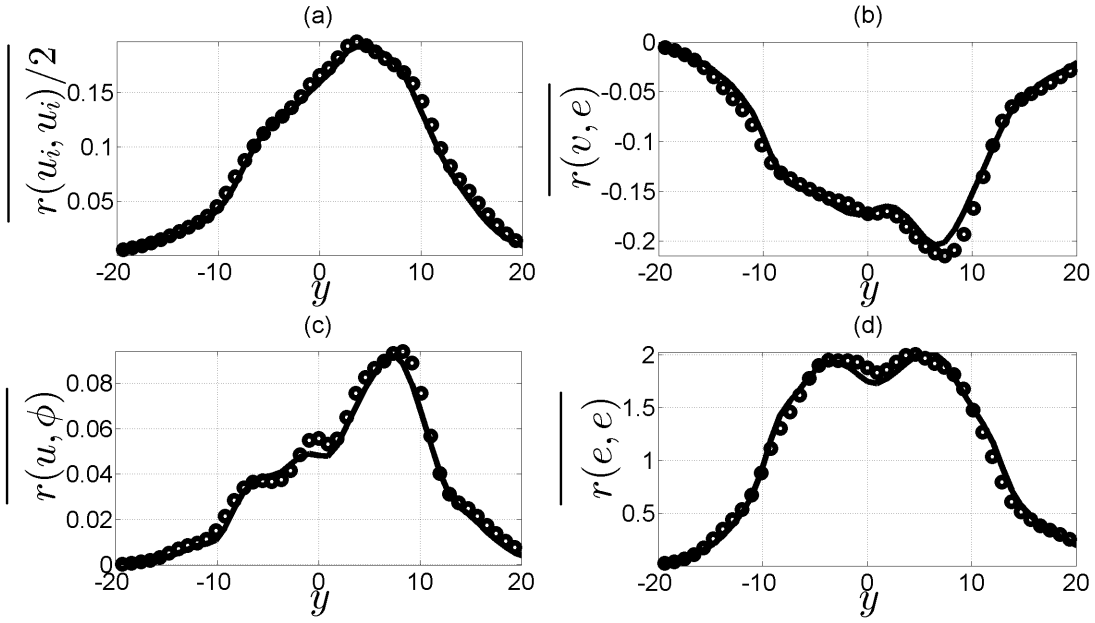

FIG. 10: Cross-stream variation of some of the components of $\overline{r}$ at $t = 65$ with $Ma = 0.6$ and $s = 2$. The thick solid line denote LES predictions using PEVC-FMDF and circles show the DNS data.

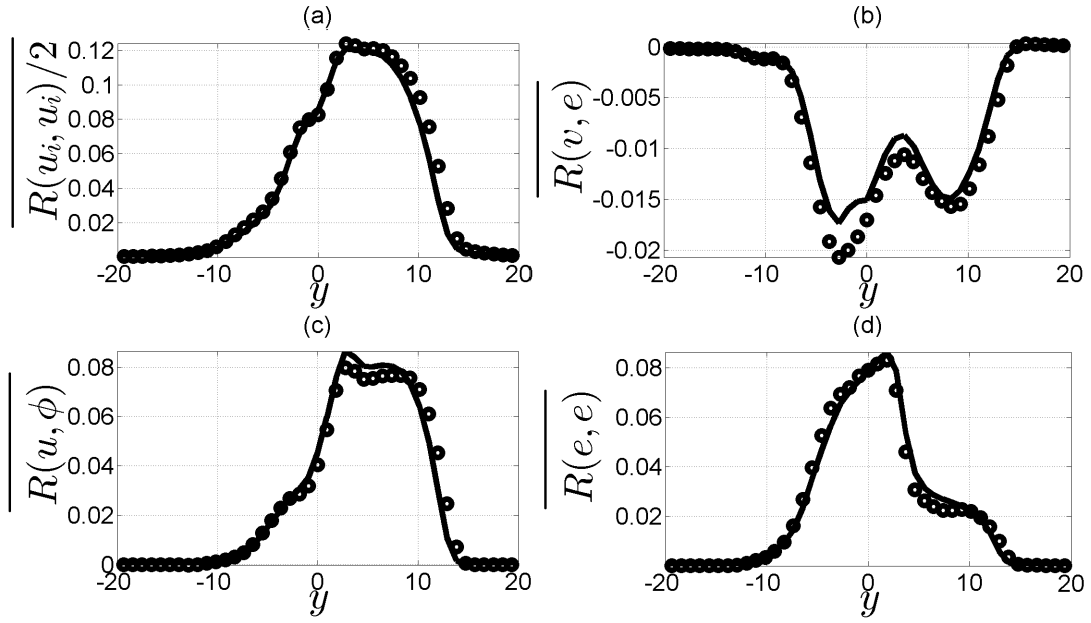

FIG. 11: Cross-stream variation of some of the components of $\overline{R}$ at $t = 75$ with $Ma = 1.2$ and $s = 2$. The thick solid line denote LES predictions using PEVC-FMDF and circles show the DNS data.

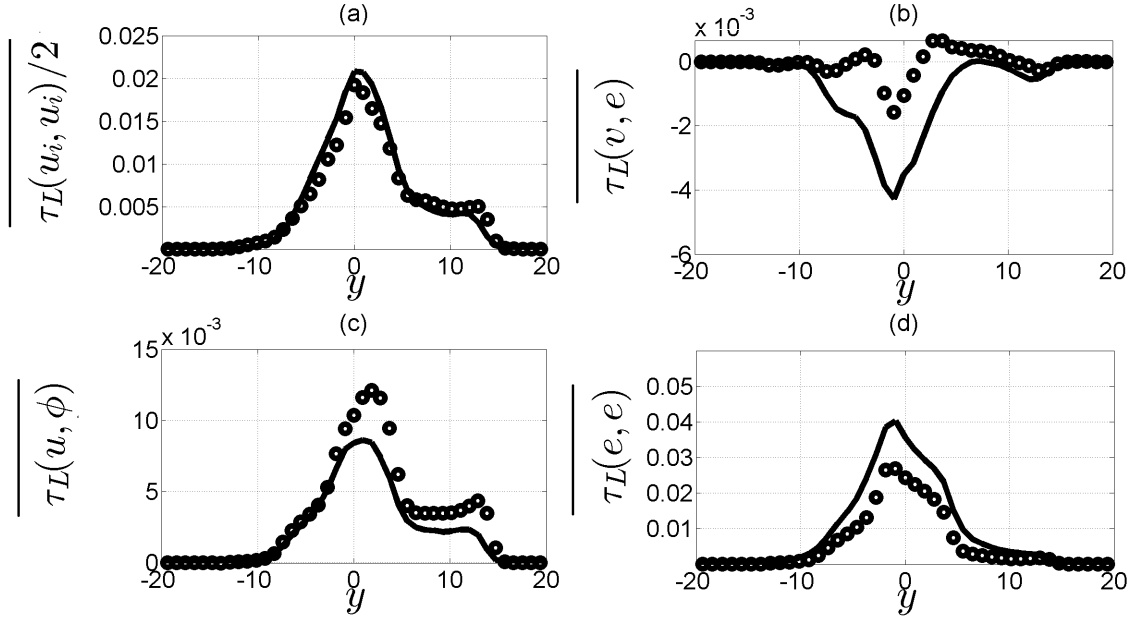

FIG. 12: Cross-stream variation of some of the Reynolds-averaged components of $\overline{\tau_L}$ at $t = 75$ with $Ma = 1.2$ and $s = 2$. The thick solid line denote LES predictions using PEVC-FMDF and circles show the DNS data.

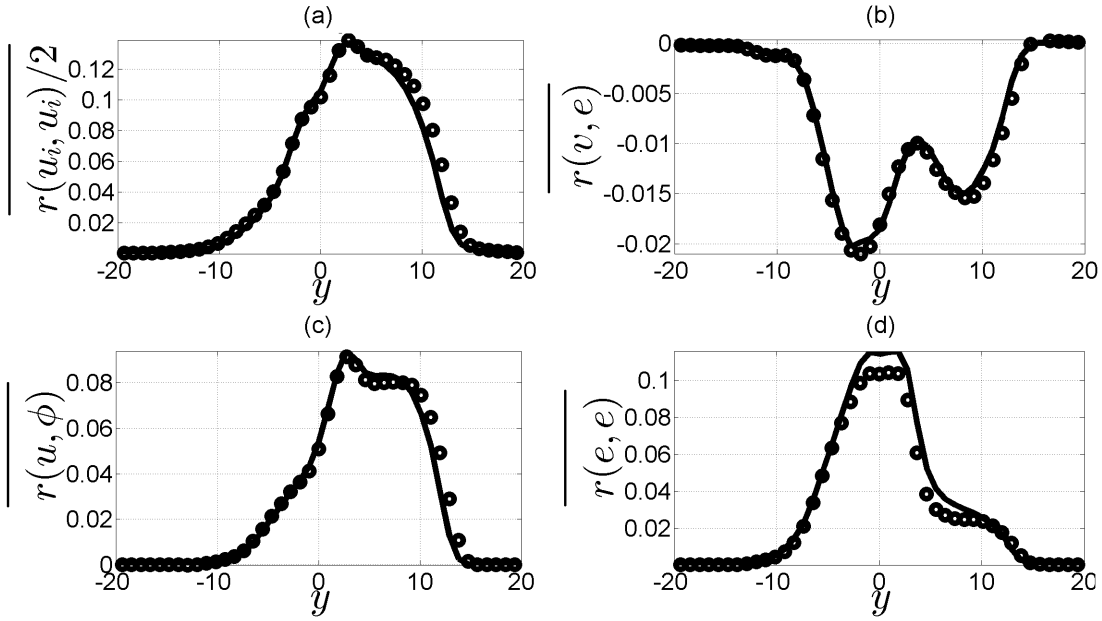

FIG. 13: Cross-stream variation of some of the components of $\overline{r}$ at $t = 75$ with $Ma = 1.2$ and $s = 2$. The thick solid line denote LES predictions using PEVC-FMDF and circles show the DNS data.

VI. SUMMARY & CONCLUSIONS

The filtered density function (FDF) has proven to be a very effective subgrid scale closure for large eddy simulation of turbulent reactive flows [2, 3]. In all previous works, the FDF were considered for selected transport variables; the closure for other variables were provided by other means. The objective of the present work is to develop the FDF in a self-contained manner, accounting for SGS statistics of all of the transport variables. For this purpose, the pressure-energy-velocity-composition filtered mass density function (PEVC-FMDF) is developed. The exact transport equation governing the evolution of this FDF is derived. It is shown that the effect of SGS convection appears in closed form. The unclosed terms are modeled in a fashion similar to that in probability density function methods. The capability of the PEVC-FMDF is demonstrated by conducting LES of a temporally developing mixing layer. The performance of the model as appraised by comparisons with DNS data is encouraging.

Future work must consider other kernels of the SLM coupled with more comprehensive SGS pressure-strain correlations, *e.g.* Refs. [88]. The same goes for developments of more sophisticated models for the terms requiring multi-point statistical information: SGS dis-

sipation, dilatation, and frequency. Extension to LES of reactive flows is straightforward if reliable kinetics models are provided. Future applications to a broader class of flows with escalated degrees of complexity are also recommended. With these extension, LES of practical flows with this self-contained FDF becomes possible, as is currently the case with scalar-FDF [39].

ACKNOWLEDGMENTS

This work is sponsored by AFOSR under Grant FA9550-12-1-0057, and by NSF under Grant CBET-1603131 and Grant CBET-1609120. Computational resources are provided by the University of Pittsburgh Center for Research Computing.

---

[1] R. S. Miller and J. W. Foster, "Survey of Turbulent Combustion Models for Large-Eddy Simulations of Propulsive Flowfields," AIAA J. **54**, 2930–2946 (2016).

[2] S. B. Pope, "Small Scales, Many Species and the Manifold Challenges of Turbulent Combustion," Proc. Combust. Inst. **34**, 1 – 31 (2013).

[3] D. C. Haworth, "Progress in Probability Density Function Methods for Turbulent Reacting Flows," Prog. Energ. Combust. **36**, 168–259 (2010).

[4] S. L. Yilmaz, N. Ansari, P. H. Pisciuneri, M. B. Nik, C. C. Otis, and P. Givi, "Applied Filtered Density Function," J. Appl. Fluid Mech. **6**, 311–320 (2013).

[5] K. K. Kuo and R. Acharya, *Fundamentals of Turbulent and Multiphase Combustion* (John Wiley and Sons Inc., Hoboken, NJ, 2012).

[6] N. Ansari, F. A. Jaberi, M. R. H. Sheikhi, and P. Givi, "Filtered Density Function as a Modern CFD Tool," in *Engineering Applications of Computational Fluid Dynamics: Volume 1*, edited by A. R. S. Maher (International Energy and Environment Foundation, 2011) Chap. 1, pp. 1–22.

[7] T. Almeida, A. Afshari, and F. A. Jaberi, "Modeling and Large-Scale Simulations of Complex Combustion Systems," in *Advances in Combustion and Noise Control*, edited by G. D. Roy, K. H. Yu, J. H. Whitelaw, and J. J. Witton (Cranfield University Press, Cranfield, England, 2006) Chap. 35, pp. 551–564.

[8] P. Givi, "Filtered Density Function for Subgrid Scale Modeling of Turbulent Combustion," AIAA J. **44**, 16–23 (2006).

[9] M. R. H. Sheikhi, P. Givi, and S. B. Pope, "Frequency-Velocity-Scalar Filtered Mass Density Function for Large Eddy Simulation of Turbulent Flows," Phys. Fluids **21**, 075102 (2009).

[10] M. B. Nik, S. L. Yilmaz, P. Givi, M. R. H. Sheikhi, and S. B. Pope, "Simulation of Sandia Flame D using Velocity-Scalar Filtered Density Function," AIAA J. **48**, 1513–1522 (2010).

[11] M. R. H. Sheikhi, P. Givi, and S. B. Pope, "Velocity-Scalar Filtered Mass Density Function for Large Eddy Simulation of Turbulent Reacting Flows," Phys. Fluids **19**, 095106 (2007).

[12] M. R. H. Sheikhi, T. G. Drozda, P. Givi, and S. B. Pope, "Velocity-Scalar Filtered Density Function for Large Eddy Simulation of Turbulent Flows," Phys. Fluids **15**, 2321–2337 (2003).

[13] M. Safari and M. R. H. Sheikhi, "Large Eddy Simulation-Based Analysis of Entropy Generation in a Turbulent Nonpremixed Flame," Energy **78**, 451–457 (2014).

[14] M. Safari, F. Hadi, and M. R. H. Sheikhi, "Progress in the Prediction of Entropy Generation in Turbulent Reacting Flows Using Large Eddy Simulation," Entropy **16**, 5159–5177 (2014).

[15] M. R. H. Sheikhi, M. Safari, and F. Hadi, "Entropy Filtered Density Function for Large Eddy Simulation of Turbulent Flows," AIAA J. **53**, 2571–2587 (2015).

[16] Z. Li, A. Banaeizadeh, and F. A. Jaberi, "Two-Phase Filtered Mass Density Function for LES of Turbulent Reacting Flows," J. Fluid Mech. **760**, 243–277 (2014).

[17] A. Irannejad and F. A. Jaberi, "Large Eddy Simulation of Turbulent Spray Combustion," Combust. Flame **162**, 431–450 (2015).

[18] L. Y. M. Gicquel, P. Givi, F. A. Jaberi, and S. B. Pope, "Velocity Filtered Density Function for Large Eddy Simulation of Turbulent Flows," Phys. Fluids **14**, 1196–1213 (2002).

[19] S. B. Pope, "Computations of Turbulent Combustion: Progress and Challenges," Proc. Combust. Inst. **23**, 591–612 (1990).

[20] P. Givi, "Model-Free Simulations of Turbulent Reactive Flows," Prog. Energ. Combust. **15**, 1–107 (1989).

[21] F. Gao and E. E. O'Brien, "A Large-Eddy Simulation Scheme for Turbulent Reacting Flows," Phys. Fluids A **5**, 1282–1284 (1993).

[22] P. J. Colucci, F. A. Jaberi, P. Givi, and S. B. Pope, "Filtered Density Function for Large Eddy Simulation of Turbulent Reacting Flows," Phys. Fluids **10**, 499–515 (1998).

[23] F. A. Jaberi, P. J. Colucci, S. James, P. Givi, and S. B. Pope, "Filtered Mass Density Function for Large-Eddy Simulation of Turbulent Reacting Flows," J. Fluid Mech. **401**, 85–121 (1999).

[24] S. L. Yilmaz, M. B. Nik, P. Givi, and P. A. Strakey, "Scalar Filtered Density Function for Large Eddy Simulation of a Bunsen Burner," J. Propul. Power **26**, 84–93 (2010).

[25] M. B. Nik, S. L. Yilmaz, M. R. H. Sheikhi, and P. Givi, "Grid Resolution Effects on VSFMDF/LES," Flow Turbul. Combust. **85**, 677–688 (2010).

[26] S. L. Yilmaz, M. B. Nik, M. R. H. Sheikhi, P. A. Strakey, and P. Givi, "An Irregularly Portioned Lagrangian Monte Carlo Method for Turbulent Flow Simulation," J. Sci. Comput. **47**, 109–125 (2011).

[27] N. Ansari, P. H. Pisciuneri, P. A. Strakey, and P. Givi, "Scalar-Filtered Mass-Density-Function Simulation of Swirling Reacting Flows on Unstructured Grids," AIAA J. **50**, 2476–2482 (2012).

[28] D. H. Rowinski and S. B. Pope, "Computational Study of Lean Premixed Turbulent Flames Using RANSPDF and LESPDF Methods," Combus. Theor. Model. **17**, 610–656 (2013).

[29] B. L. Sawford, S. B. Pope, and P. K. Yeung, "Gaussian Lagrangian Stochastic Models for Multi-Particle Dispersion," Phys. Fluids **25**, 055101 (2013).

[30] A. Banaeizadeh, A. Afshari, H. Schock, and F. A. Jaberi, "Large Eddy Simulations of Turbulent Flows in Internal Combustion Engines," Int. J. Heat Mass Tran. **60**, 781–796 (2013).

[31] P. H. Pisciuneri, S. L. Yilmaz, P. A. Strakey, and P. Givi, "An Irregularly Portioned FDF Simulator," SIAM J. Sci. Comput. **35**, C438–C452 (2013).

[32] Y. Yang, H. Wang, S. B. Pope, and J. H. Chen, "Large-Eddy Simulation/Probability Density Function Modeling of a Non-Premixed CO/H2 Temporally Evolving Jet Flame," Proc. Combust. Inst. **34**, 1241–1249 (2013).

[33] J. Kim and S. B. Pope, "Effects of Combined Dimension Reduction and Tabulation on the Simulations of a Turbulent Premixed Flame Using a Large-Eddy Simulation/Probability Density Function Method," Combust. Theo. Model. **18**, 388–413 (2014).

[34] J. Minier, S. Chibbaro, and S. B. Pope, "Guidelines for the Formulation of Lagrangian Stochastic Models for Particle Simulations of Single-Phase and Dispersed Two-Phase Turbulent Flows," Phys. Fluids **26**, 113303 (2014).

[35] P. P. Popov and S. B. Pope, "Large Eddy Simulation/Probability Density Function Simulations of Bluff Body Stabilized Flames," Combust. Flame **161**, 3100–3133 (2014).

[36] I. A. Dodoulas and S. Navarro-Martinez, "Analysis of Extinction in a Non-Premixed Turbulent Flame Using Large Eddy Simulation and the Chemical Explosion Mode Analysis," Combust. Theo. Model. **19**, 107–129 (2015).

[37] W. P. Jones, A. J Marquis, and D. Noh, "LES of a Methanol Spray Flame with a Stochastic Sub-Grid Model," Proc. Combust. Inst. **35**, 1685–1691 (2015).

[38] P. H. Pisciuneri, S. L. Yilmaz, P. A. Strakey, and P. Givi, "Massively Parallel FDF Simulation of Turbulent Reacting Flows," in *Stochastic Equations for Complex Systems: Theoretical and Computational Topics*, Mathematical Engineering, edited by S. Heinz and H. Bessaih (Springer, 2015) Chap. 8, pp. 175–192.

[39] N. Ansari, P. A. Strakey, G.M. Goldin, and P. Givi, "Filtered Density Function Simulation of a Realistic Swirled Combustor," Proc. Combust. Inst. **35**, 1433–1442 (2015).

[40] M. Esmaelli, A. Afshari, and F. A. Jaberi, "Turbulent Mixing in Non-Isothermal Jet in Cross-Flow," Int. J. Heat Mass Tran. **89**, 1239–1257 (2015).

[41] Y. Liang, S. B. Pope, and P. Pepiot, "A Pre-Partitioned Adaptive Chemistry Methodology for the Efficient Implementation of Combustion Chemistry in Particle PDF Methods," Combust. Flame **162**, 3236–3253 (2015).

[42] S. Sammak, A. G. Nouri, N. Ansari, and P. Givi, "Quantum Computing and Its Potential for Turbulence Simulations," in *Mathematical Modeling of Technological Processes*, Communications in Computer and Information Science, edited by N. Danaev, Y. Shokin, and D. Akhmed-Zakin (Springer, 2015) Chap. 13, pp. 124–132.

[43] S. Sammak, M. J. Brazell, P. Givi, and D. J. Mavriplis, "A Hybrid DG-Monte Carlo FDF Simulator," Comput. Fluids **140**, 158–166 (2016).

[44] R. R. Tirunagari and S. B. Pope, "LES/PDF for Premixed Combustion in the DNS Limit," Combust. Theo. Model. **20**, 1–32 (2016).

[45] S. Sammak, A. G. Nouri, M. J. Brazell, D. J. Mavriplis, and P. Givi, "Discontinuous Galerkin-Monte Carlo Solver for Large Eddy Simulation of Compressible Turbulent Flows," in *55th AIAA Aerospace Sciences Meeting* (AIAA, Grapevine, TX, 2017) AIAA-2017-0982.

[46] R. R. Tirunagari and S. B. Pope, "An Investigation of Turbulent Premixed Counterflow Flames Using Large-Eddy Simulations and Probability Density Function Methods," Combust. Flame **166**, 229–242 (2016).

[47] A. G. Nouri, S. Sammak, P. H. Pisciuneri, and P. Givi, "Langevin Simulation of Turbulent Combustion," in *Combustion for Power Generation and Transportation: Technology, Challenges and Prospects*, edited by A. K. Agarwal, S. De, A. Pandey, and A. P. Singh (Springer, Singapore, 2017) pp. 39–53.

[48] W. P. Jones, A. J. Marquis, and D. Noh, "A Stochastic Breakup Model for Large Eddy Simulation of a Turbulent Two-Phase Reactive Flow," Proc. Combust. Inst. **36**, 2559–2566 (2017).

[49] A. Banaeizadeh, Z. Li, and F. A. Jaberi, "Compressible Scalar Filtered Density Function Model for High-Speed Turbulent Flows," AIAA J. **49**, 2130–2143 (2011).

[50] M. B. Nik, P. Givi, C. K. Madnia, and S. B. Pope, "EPVS-FMDF for LES of High-Speed Turbulent Flows," in *50th AIAA Aerospace Sciences Meeting Including the New Horizons Forum and Aerospace Exposition* (AIAA, Nashville, TN, 2012) AIAA-2012-0117.

[51] T. G. Drozda, J. R. Quinlan, P. H. Pisciuneri, and S. L. Yilmaz, "Progress Toward Affordable High Fidelity Combustion Simulations for High-Speed Flows in Complex Geometries," in *48th AIAA/ASME/SAE/ASEE Joint Propulsion Conference and Exhibit and 10th International Energy Conversion Engineering Conference* (AIAA, Atlanta, GA, 2012) AIAA-2012-4264.

[52] P. A. Libby and F. A. Williams, *Turbulent Reacting Flows*, Topics in Applied Physics, Vol. 44 (Springer-Verlag, Heidelberg, 1980).

[53] S. B. Pope, "PDF Methods for Turbulent Reactive Flows," Prog. Energ. Combust. **11**, 119–192 (1985).

[54] R. W. Bilger, "Molecular Transport Effects in Turbulent Diffusion Flames at Moderate Reynolds Number," AIAA J. **20**, 962–970 (1982).

[55] T. Poinsot and D. Veynante, *Theoretical and Numerical Combustion*, 3rd ed. (R. T. Edwards, Inc., Bordeaux, France, 2012).

[56] S. B. Pope, *Turbulent Flows* (Cambridge University Press, Cambridge, U.K., 2000).

[57] U. Piomelli, "Large-Eddy Simulation: Achievements and Challenges," Prog. Aerosp. Sci. **35**, 335–362 (1999).

[58] C. Meneveau and J. Katz, "Scale-Invariance and Turbulence Models for Large-Eddy Simulation," Annu. Rev. Fluid Mech. **32**, 1–32 (2000).

[59] B. J. Geurts, *Modern Simulation Strategies for Turbulent Flow* (R. T. Edwards, Inc., Philadelphia, PA, 2001).

[60] P. Sagaut, *Large Eddy Simulation for Incompressible Flows*, 3rd ed. (Springer-Verlag, New York, NY, 2005).

[61] M. Germano, "Turbulence: the Filtering Approach," J. Fluid Mech. **238**, 325–336 (1992).

[62] E. E. O'Brien, "The Probability Density Function (PDF) Approach to Reacting Turbulent Flows," in *Turbulent Reacting Flows*, Topics in Applied Physics, Vol. 44, edited by Paul Libby and Forman Williams (Springer, Heidelberg, 1980) Chap. 5, pp. 185–218.

[63] B. Vreman, B. Geurts, and H. Kuerten, "Realizability Conditions for the Turbulent Stress Tensor in Large-Eddy Simulation," J. Fluid Mech. **278**, 351–362 (1994).

[64] N. Wax, *Selected Papers on Noise and Stochastic Processes* (Dover, 1954).

[65] B. J. Delarue and S. B. Pope, "Application of PDF Methods to Compressible Turbulent Flows," Phys. Fluids **9**, 2704–2715 (1997).

[66] B. J. Delarue and S. B. Pope, "Calculations of Subsonic and Supersonic Turbulent Reacting Mixing Layers Using Probability Density Function Methods," Phys. Fluids **10**, 487–498 (1998).

[67] D. C. Haworth and S. B. Pope, "A Generalized Langevin Model for Turbulent Flows," Phys. Fluids **29**, 387–405 (1986).

[68] T. D. Dreeben and S. B. Pope, "Probability Density Function and Reynolds-Stress Modeling of Near-Wall Turbulent Flows," Phys. Fluids **9**, 154–163 (1997).

[69] C. Dopazo and E. E. O'Brien, "Statistical Treatment of Non-Isothermal Chemical Reactions in Turbulence," Combust. Sci. Technol. **13**, 99–122 (1976).

[70] M. P. Martin, U. Piomelli, and G. V. Candler, "Subgrid-Scale Models for Compressible Large-Eddy Simulations," Theor. Comp. Fluid Dyn. **13**, 361–376 (2000).

[71] H. Risken, *The Fokker-Planck Equation, Methods of Solution and Applications* (Springer-Verlag, New York, NY, 1989).

[72] M. Muradoglu, S.B. Pope, and D. A. Caughey, "The Hybrid Method for the PDF Equations of Turbulent Reactive Flows: Consistency Conditions and Correction Algorithms," J. Comput. Phys. **172**, 841–878 (2001).

[73] P. E. Kloeden, E. Platen, and H. Schurz, *Numerical Solution of Stochastic Differential Equations through Computer Experiments*, 2nd ed. (Springer, Berlin; New York, 1997).

[74] I. I. Gikhman and A. V. Skorokhod, *Stochastic Differential Equations* (Springer-Verlag, New York, NY, 1972).

[75] M. Muradoglu, P. Jenny, S. B. Pope, and D. A. Caughey, "A Consistent Hybrid Finite-Volume/Particle Method for the PDF Equations of Turbulent Reactive Flows," J. Comput. Phys. **154**, 342–371 (1999).

[76] P. A. McMurtry, W.-H. Jou, J. J. Riley, and R. W. Metcalfe, "Direct Numerical Simulations of a Reacting Mixing Layer with Chemical Heat Release," AIAA J. **24**, 962–970 (1986).

[77] R. D. Moser and M. M. Rogers, "The Three-Dimensional Evolution of a Plane Mixing Layer: Pairing and Transition to Turbulence," J. Fluid Mech. **247**, 275–320 (1993).

[78] B. Vreman, B. Geurts, and H. Kuerten, "Large-Eddy Simulation of the Turbulent Mixing Layer," J. Fluid Mech. **339**, 357–390 (1997).

[79] T. J. Poinsot and S. K. Lele, "Boundary Conditions for Direct Simulations of Compressible Viscous Flows," J. Comput. Phys. **101**, 104–129 (1992).

[80] G. Erlebacher, M. Y. Hussaini, C. G. Speziale, and T. A. Zang, "Toward the Large-Eddy Simulation of Compressible Turbulent Flows," J. Fluid Mech. **238**, 155–185 (1992).

[81] S. B. Pope, "Ten Questions Concerning the Large-Eddy Simulation of Turbulent Flows," New J. Phys. **6**, 35 (2004).

[82] J. Giridhar, *A Framework for Large Eddy Simulation of Incompressible Flows with Error Control*, Ph.D. Thesis, Sibley School of Mechanical and Aerospace Engineering, Cornell University, Ithaca, NY (2005).

[83] S. B. Pope, "On the Relation Between Stochastic Lagrangian Models of Turbulence and Second-Moment Closures," Phys. Fluids **6**, 973–985 (1994).

[84] R. W. Metcalfe, S. A. Orszag, M. E. Brachet, S. Menon, and J. J. Riley, "Secondary Instabilities of a Temporally Growing Mixing Layer," J. Fluid Mech. **184**, 207–243 (1987).

[85] C. Pantano and S. Sarkar, "A Study of Compressibility Effects in the High-Speed Turbulent Shear Layer Using Direct Simulation," J. Fluid Mech. **451**, 329–371 (2002).

[86] A. W. Vreman, N. D. Sandham, and K. H. Luo, "Compressible Mixing Layer Growth Rate and Turbulence Characteristics," J. Fluid Mech. **320**, 235–258 (1996).

[87] P. Givi, C. K. Madnia, C. J. Steinberger, M. H. Carpenter, and J. P. Drummond, "Effects of Compressibility and Heat Release in a High Speed Reacting Mixing Layer," Combust. Sci. Technol. **78**, 33–68 (1991).

[88] A. A. Mishra and S. S. Girimaji, "On The Realizability Of Pressure-Strain Closures," J. Fluid Mech. **755**, 535–560 (2014).